ACS APPLIED MATERIALS & INTERFACES

Research Article

www.acsami.org

Platinum Electrodeposition at Unsupported Electrochemically Reduced Nanographene Oxide for Enhanced Ammonia Oxidation

Lisandro Cunci,[†] Carlos A. Velez,[†] Ivan Perez,[†] Amal Suleiman,[†] Eduardo Larios,[‡,⊥] Miguel José-Yacamán,[‡] James J. Watkins,[§] and Carlos R. Cabrera*[,†]

[†]Department of Chemistry and Center for Advanced Nanoscale Materials, University of Puerto Rico, Río Piedras Campus, P.O. Box 23346, San Juan, Puerto Rico 00931-3346, United States

[‡]Physics and Astronomy Department, University of Texas at San Antonio, San Antonio, Texas 78249, United States

[§]Department of Chemical Engineering, University of Massachusetts, Amherst, Massachusetts 01003, United States

[⊥]Departamento de Ingeniería Química, Universidad de Sonora, 83000 Hermosillo, Sonora, México

ABSTRACT: The electrochemical reduction of highly oxidized unsupported graphene oxide nanosheets and its platinum electrodeposition was done by the rotating disk slurry electrode technique. Avoiding the use of a solid electrode, graphene oxide was electrochemically reduced in a slurry solution with a scalable process without the use of a reducing agent. Graphene oxide nanosheets were synthesized from carbon platelet nanofibers to obtain highly hydrophilic layers of less than 250 nm in width. The graphene oxide and electrochemically reduced graphene oxide/Pt (erGOx/Pt) hybrid materials were characterized through different spectroscopy and microscopy techniques. Pt nanoparticles with 100 facets, clusters, and atoms at erGOx were identified by high resolution transmission electron microscopy (HRTEM). Cyclic voltammetry was used to characterize the electrocatalytic activity of the highly dispersed erGOx/Pt hybrid material toward the oxidation of ammonia, which showed a 5-fold current density increase when compared with commercially available Vulcan/Pt 20%. This is in agreement with having Pt (100) facets present in the HRTEM images of the erGOx/Pt material.

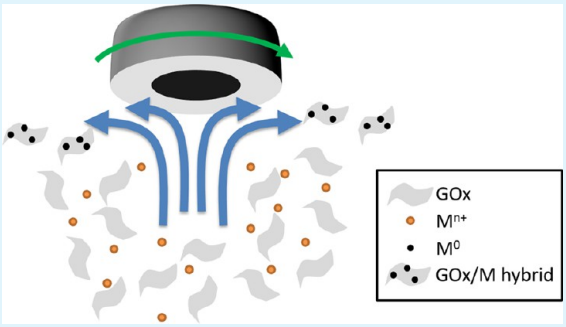

KEYWORDS: *Graphene, ammonia oxidation, platinum, RoDSE, unsupported electrodeposition*

1. INTRODUCTION

Hummers and Offeman stated, in 1958, the most used procedure to exfoliate graphite particles into graphene oxide (GOx),[1] which separates the carbon sp^2 layers by oxidizing the carbon atoms to sp^3 with oxygen functionalities. This, in turn, can be reduced to graphene, which was believed to be unstable until 2004, when K. S. Novoselov and A. K. Geim, 2010 Nobel Laureates, showed that it can be isolated by simply sticking and unsticking tape to graphite until only one layer is separated from the rest and placed in another surface.[2,3] Since then, graphene has been explored for practical applications. As the only two-dimensional material (one atom thick) known until now, all its volume is at its surface, having a theoretical surface area of 2630 m^2/g, and specific surface area values reported much higher than that for Vulcan XC-72, the most commonly used carbon support.[4]

This increasingly high interest in graphene since 2004 is due to its outstanding properties such as high conductivity and high surface area.[5] In the last 6 years, graphene has been described as a promising material due to its ease of preparation, low cost potential, metallic conductivity (ballistic) at room temperature, and low electric noise.[6] These properties are changed by the addition of oxygenated functional groups (i.e., carbonyl, carboxyl, hydroxyl, etc.) when using GOx, because these groups alter the continuity of its electron density.[7,8] GOx is easily synthesized,[9] and the high concentration of carbon−oxygen moieties on both surfaces provide a large amount of nucleation sites to deposit metal catalyst nanoparticles. GOx can also be reduced to what is known as reduced graphene oxide (erGOx), maintaining reasonable conductivity and transparency for applications such as sensors[10] and ultrathin films.[11]

GOx has been widely used as a catalyst support for several metal catalysts such as Pt,[12−14] Au,[15] Co,[16] Pd,[17] Fe,[18] and alloys.[12] Several deposition techniques have been used to synthesize the GOx/metal hybrids such as chemical reduction (e.g., hydrazine,[13] $NaBH_4$,[19] etc.), sol−gel synthesis,[12] and microwave-assisted chemical reduction,[20] among others. Electrochemical depositions have also been done where the GOx/metal hybrid is deposited onto a solid electrode.[21] However, to the best of our knowledge, no electrochemical synthesis of an electrochemical reduced GOx/Pt hybrid

Received: November 20, 2013
Accepted: January 13, 2014
Published: January 13, 2014

   dx.doi.org/10.1021/am4052552 | *ACS Appl. Mater. Interfaces* 2014, 6, 2137−2145

material has been done on unsupported GOx. Rotating disk slurry electrode (RoDSE) is a technique developed by our laboratory where isolated atoms, clusters, and metal nanoparticles are deposited onto an unsupported nanocarbon material.[22−24] This technique has been proven in other carbonaceous supports such as Vulcan XC-72,[22] nanotubes,[23] and nano-onions,[24] but it has not been used with GOx.

The interest in the oxidation of ammonia has increased due to alkaline ammonia fuel cells, wastewater treatment, and its high capacity for hydrogen storage. Pt (100) surfaces have been known to be the most efficient electrocatalyst to oxidize ammonia.[25,26] The most widely accepted mechanism for the ammonia oxidation in basic media on polycrystalline platinum surfaces was proposed by Gerischer and Mauerer.[27,28] The proposed mechanism leads to nitrogen gas formation from ammonia through a sequential series of reactions shown below:

$$NH_3(aq) \rightarrow NH_{3,ads} \quad (1)$$

$$NH_{3,ads} \leftrightarrow NH_{2,ads} + H^+ + e^- \quad (2)$$

$$NH_{2,ads} \rightarrow NH_{ads} + H^+ + e^- \quad (3)$$

$$NH_{x,ads} + NH_{y,ads} \rightarrow N_2(g) + (x + y)H^+ + (x + y)e^- \quad (4)$$

$$NH_{ads} \rightarrow N_{ads} + H^+ + e^- \quad (5)$$

$$N_{ads} + N_{ads} \rightarrow N_2(g) \quad (6)$$

In this work, the electrochemically reduced GOx/Pt hybrid material was characterized through different spectroscopy and microscopy techniques, and its electrocatalytic activity toward ammonia oxidation was studied by cyclic voltammetry and compared to commercial available Vulcan/20%Pt and polycrystalline Pt disk electrodes.

2. EXPERIMENTAL SECTION

2.1. Synthesis of GOx. High quality GOx nanosheets were prepared by a slight modification of a synthesis reported by D. C. Marcano et al.[9] to increase the oxidation and dispersion in aqueous solutions. Briefly, 100 mg of graphite platelet nanofibers (Sigma-Aldrich) were dispersed by sonication in 40 mL of (9:1) H_2SO_4 and H_2PO_4. After complete dispersion, the mixture was stirred vigorously while 600 mg (6 times the weight of graphite) of $KMnO_4$ was slowly added. The temperature was set to 50 °C, and the mixture was left stirring for 18 h. Then, the solution was poured slowly into 400 mL of ice-cold 18.2 MΩ cm dionized water while stirring. In addition, 6 mL of H_2O_2 (35% in water) was added dropwise until the solution turned bright yellow. The solution was then heated until boiling, which turned the solution brown again, and it was filtered with a 0.8 μm Nylon filter.

After filtering, the brown slurry was dispersed in an 84 mL mixture of water and DMF by sonication. The solution was divided into six centrifugation tubes and centrifuged at 3400 rpm for 8 min. The supernatant was extracted, dispersed in abundant water, and filtered with a 0.1 μm polycarbonate filter. The filtered material was dried under vacuum at room temperature and grinded to fine powder, which was used for further characterization and electrochemical studies.

2.2. Synthesis of GOx/Pt Hybrid Material by RoDSE Technique. The erGOx/Pt nanocatalysts preparation was done by using the RoDSE technique.[22] The suspension was made in a beaker with 28.48 mg of graphene and 20 mL of 0.1 M H_2SO_4 (Optima Aldrich) and maintained under ultrasound for 30 min. The formed slurry suspension was inserted in the center of a three-electrode cell assembly for the platinum electrodeposition under hydrodynamic conditions using the rotating glassy carbon (GC) disk electrode (RDE). The three electrochemical cell compartments were isolated by glass frits. At the center compartment, 2.00 mL of a 5 mM K_2PtCl_6 (Aldrich) solution was added to the slurry suspension. The electrochemical cell was sealed and purged with Argon (to remove all atmospheric gas that may interfere with the nanocatalytic particles preparation) for 30 min, whereas the RDE (PINE Instrument Co.) rotated at 900 rpm in the slurry solution of graphene and H_2SO_4. The GC RDE, with a 0.20 cm^2 geometric area was used as the working electrode. A graphite rod and Ag|AgCl electrode were used as counter and reference electrodes, respectively. The Pt electrodeposition for the formation of erGOx/Pt hybrid material was done by applying a constant potential of −0.200 V vs Ag/AgCl for 2.0 h using a Basic Electrochemical System from EG&G. The chronoamperometry process was repeated three additional times with the addition of 2.00 mL of 5 mM K_2PtCl_6 in each repetition. Finally, the slurry solution was filtrated and rinsed with 900 mL of deionized water (18.2 MΩ cm, Nanopure Diamond, Barnstead).

2.3. Characterization Techniques. A Carl Zeiss LEO 922 TEM system was used for the transmission electron microscopy (TEM) images, operated with an accelerating voltage of 200 kV. For high resolution scanning transmission electron microscopy (HRSTEM) images was used a JEOL JEM-ARM200F electron microscope. HRSTEM images were simultaneously recorded in both the high angle annular dark field (HAADF) and bright field (BF) modes with the microscope operated at 200 kV. The probe correction was performed with a CEOS corrector obtaining a 12-fold Ronchigram with a flat area of ∼50 mrad. The images were registered with a condenser lens aperture of 40 μm, HAADF collection angle ranges from 50 to 180 mrad, and the spot size used was ∼23.2 pA. X-ray diffraction (XRD) patterns were obtained on a PANalytical X'Pert material research diffractometer operating with the Cu Kα radiation (λ = 1.54 Å). Micro-Raman scattering experiments were performed using a Jobin Yvon Horiba LabRam HR 800 Raman microscope with a laser source with a wavelength of 632 nm. IR spectra were obtained in a Perkin-Elmer ATR FT-IR with a resolution of 4 cm^{-1}. X-ray photoelectron spectroscopy (XPS) spectra were obtained using a PHI QUANTUM spectrometer equipped with an Al Kα monochromatic X-ray source at a grazing angle of 10°. A pass energy of 58.70 eV was used. All the binding energies reported were corrected fixing the carbon peak (C 1s) at 284.5 eV.

2.4. Electrochemical Measurements. The electrodes were prepared by two different methods: (1) the ink−paste method, described elsewhere[29] and (2) the capillary electrode method. In general, in the ink−paste method, 1 mg of the catalyst to be tested was added to 50 μL of deionized H_2O and, after sonication, 150 μL of isopropanol and 2.7 μL of a Nafion solution of 5% dispersion in lower aliphatic alcohols (Aldrich) were added to the paste. The mixture was placed under ultrasound conditions until full dispersion was reached. This was followed by placing 10 μL of the ink on different GC electrodes (BAS Inc.) and air-dried. In the latter method, a glass capillary was filled in one end with a graphite-based paste (a mixture of graphite powder and mineral oil), and a copper wire was introduced through the other end of the capillary, and it was allowed to air-dry overnight. Then, the capillary end with the carbon paste was pressed against the catalyst powder material several times until the graphite-based pasted capillary tip side was completely filled. The electrochemical measurements were done using a three-electrode electrochemical cell equipped with catalyst coated GC or the catalyst filled capillary working electrodes. A Pt wire and a Ag|AgCl electrode (BAS Inc.) were used as counter and reference electrodes, respectively. All cyclic voltammetric electrochemical measurements were done with an Autolab (PGSTAT 30) potentiostat.

3. RESULTS AND DISCUSSION

3.1. GOx Synthesis and Characterization. To synthesize small GOx layers, carbon platelet nanofibers were chosen due to the small size of their basal plane (200), with diameter of up to 250 nm. The smaller size of the GOx has two principal roles: (1) it increases the hydrophilicity, which helps the layers to stay in solution longer, and (2) it makes it harder for the layers to

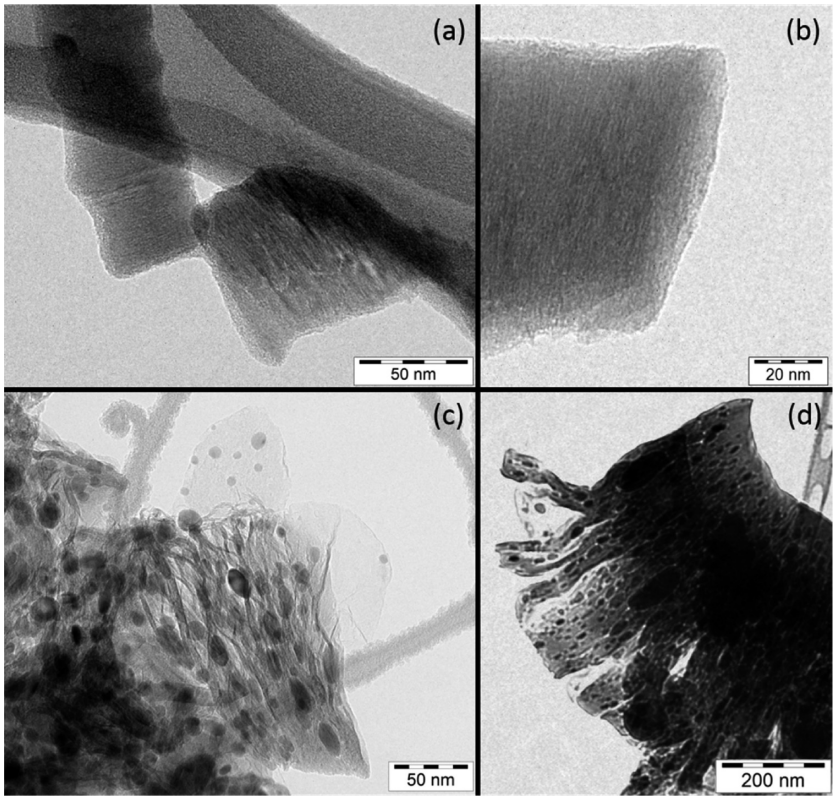

Figure 1. Transmission electron microscopy images of (a) graphite carbon platelet nanofibers with (b) close-up, and preGOx where (c) single and (d) multiple layers can be seen.

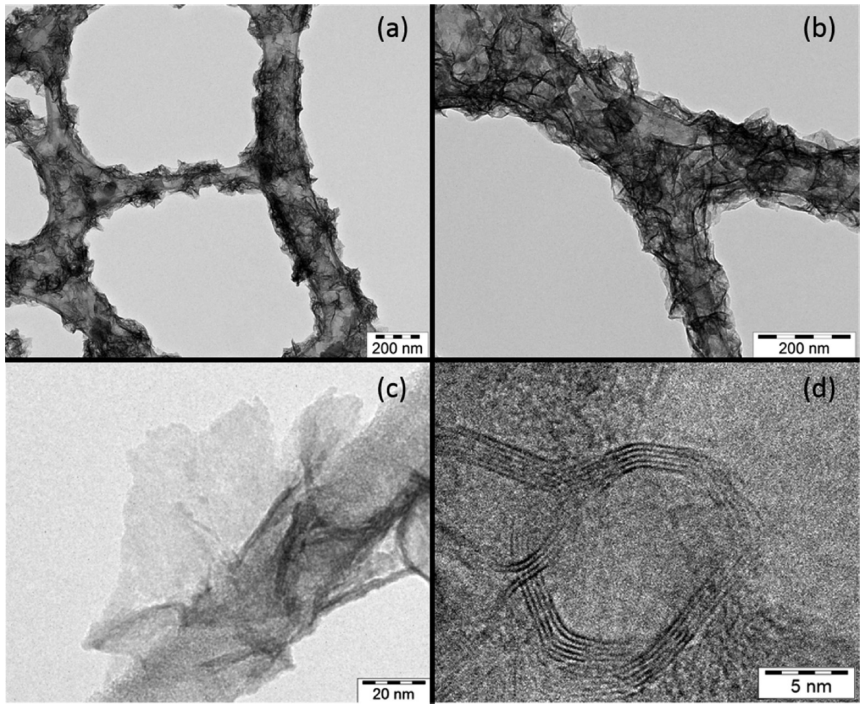

Figure 2. Transmission electron microscopy images of highly hydrophilic GOx (a, b) wrapped around carbon fibers, (c) single, and (d) multiple layers.

fold-in and avoids covering the metal nanoparticles, which produces a loss of active area for catalysis. Figure 1a,b shows TEM images of carbon platelet nanofibers of about 50 and 80 nm diameters where the basal plane can be seen as parallel lines across the fibers. The GOx obtained after the first filtration did not stay suspended in nanopure water long enough for the electrodeposition in aqueous solution. Nevertheless, GOx obtained after the last filtration stayed suspended in aqueous solution for days. Hence, the mixing of GOx in a DMF/H_2O solution and ultrasonication improved the separation of GOx

dx.doi.org/10.1021/am4052552 | *ACS Appl. Mater. Interfaces* 2014, 6, 2137−2145

nanolayers, a crucial step for the GOx to be used with the RoDSE technique in an aqueous solution. This better separation of the layers may be due to the interaction that DMF can have with the areas of the GOx that have sp^2 hybridization, which cannot occur with H_2O. A sample was obtained during the GOx synthesis before the addition of H_2O_2 and sonication (preGOx), which is shown in Figure 1c,d. Partially exfoliated GOx layers can be seen together with dark nanoparticles due to the potassium permanganate used in the process. The final GOx layers are very small, highly oxidized, and therefore, highly hydrophilic. This can be clearly seen in Figure 2a,b, which shows GOx single layers wrapped around the carbon net in a Lacey Carbon TEM grid (Ted Pella, Inc.). A single GOx layer of about 100 nm diameter can be seen in Figure 2c, next to the carbon fiber in the TEM grid. Not only was single layer GOx found in the sample but also multilayer GOx, as can be seen in Figure 2d in the HRTEM image where the dark lines are GOx layers, which were found stacked in different amounts. After obtaining a highly dispersed solution of GOx, the RoDSE technique was used for the electrodeposition of Pt.

3.2. RoDSE Electrodeposition. In the RoDSE technique, a metal precursor is dissolved into a dispersed in a slurry solution of a colloidal support, and an electrodeposition potential is applied to the RDE while rotating at 900 rpm. Figure 3 shows a scheme of the RoDSE process where the convection generated in the solution due to rotation of the RDE attracts the GOx layers toward the disk where the metal is electrodeposited on the GOx. The Pt electrodeposition may be happening by two mechanisms: the electrochemical reduction of Pt salts when the metal ions are close to the electrode and the GOx layers, or the GOx layers may get charged when they are close to the electrode and, as they move away, Pt ions can be reduced due to this charged GOx layer.

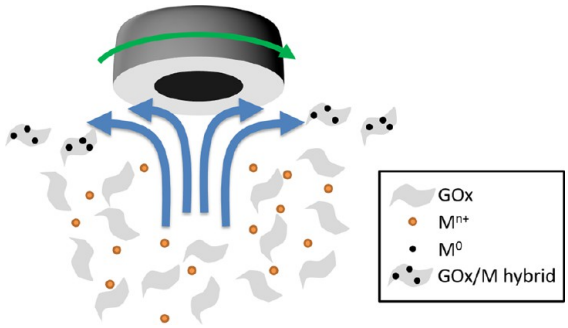

Figure 3. Schematic of the RoDSE technique process.

One important consideration for the carbon support to be used with this technique is that it should stay dispersed in an aqueous solution without settling down during the time of the electrodeposition; otherwise, the solution becomes depleted of the support material and a completely inhomogeneous material is synthesized. GOx is hydrophilic in general terms due to the oxygenated functionalities, which interact by hydrogen bonding and dipole−dipole forces with water molecules. However, its hydrophilicity and the time that takes GOx layers to settle down in aqueous solutions greatly depend on its size. A vast part of the GOx area still has sp^2 carbon bonds, which makes those areas hydrophobic. The relationship between the amount of sp^2 bonds and carbon−oxygen functionalities is related to its time suspended in solution because the more functionalities, the longer it stays suspended in polar liquids such as water. Moreover, because the GOx edges are populated with carboxyl groups, the smaller the GOx layers (more edge per layer area), the more hydrophilic they are, and the more it takes for them to settle down.[30]

3.3. erGOx/Pt Characterization. *3.3.1. XPS.* The XPS full binding energy spectra for graphite, GOx, and erGOx/Pt are shown in Figure 4a. The oxygen binding energy peak (O1s) clearly appears after the synthesis of the GOx due to the highly oxidative treatment used for the exfoliation of the graphite nanofibers. Oxygen Auger KLL peaks also appeared at higher binding. The elemental C/O ratio for the GOx and the erGOx/Pt samples were 1.96 and 2.57, respectively, which means that the GOx was also reduced during the electrodeposition using the RoDSE method.

Figure 4b shows the C1s peaks with the dashed line showing 284.5 eV, where the peak for the sp^2 carbon in graphite is located. In GOx, the carbon−oxygen moieties added a peak at a higher binding energy constructed by the convolution of the C—O, C—O—C, C═O, and O—C═O peaks. The achievement of the high oxidation state of GOx, needed for a good dispersion in aqueous solutions, is supported by the higher carbon−oxygen binding energy peak area compared to the carbon sp^2 peak. Moreover, the RoDSE process clearly reduces the carbons in the GOx, as seen for the lower carbon−oxygen peak compared to the carbon sp^2 peak. In addition, the carbon sp^2 peak is displaced to higher binding energy in GOx due to the electro-attracting forces exerted by the high amount of oxygen bonded to the carbon. However, due to the highly dispersed atomic Pt deposition, the carbon peak in the erGOx/Pt is displaced to lower binding energy because of the highly available electron density donated by the Pt atoms. The carbon sp^2 peaks are also broader compared to graphite, which may be explained by the inconsistent amount of oxygen and platinum interacting with the different carbons along the GOx and erGOx supports. The O1s peaks for the GOx and erGOx/Pt are shown in Figure 4c where addition of the Pt atoms to the support displaces the O1s peak to lower binding energies, as happened with the C1s peak.

Figure 4d shows the $Pt4f_{5/2}$ and $Pt4f_{7/2}$ peaks with their deconvolution. A mixture of Pt^0, Pt^{2+}, and Pt^{4+} atoms are found in erGOx/Pt after the sample was thoroughly washed during the filtering. These Pt^{2+} and Pt^{4+} ions can be a mixture of the precursor salts, which were not washed out during filtering, although Cl peaks are not seen, and ions attached to oxygen atoms, which are the ones interacting and displacing the oxygen 1s peak toward lower binding energies. Pt^0 is known to be the best catalyst for the oxidation of ammonia; however, no studies have been done whether Pt ions can add to this reaction.

3.3.2. Raman Spectroscopy. Raman was used to study the synthesis of GOx and its change in erGOx/Pt. The spectra of GOx and erGOx/Pt are shown in Figure 5a. There was no change between the Raman spectra of GOx and erGOx/Pt, which had the G peak at 1599 cm^{-1} and the D peak at 1342 cm^{-1}. Although the G peak is characteristic of graphite, the D peak is associated to the amount of defects in graphene oxide. As explained above, GOx was synthesized with the aim of less than 250 nm wide layers, which implied a higher amount of borders per sample, thus expecting the bigger D peak. The 2D peak is a convolution of several peaks corresponding to different amount of layers. Because no changes were done to the GOx structure during the Pt electrodeposition, the Raman spectra, before and after the deposition, did not change.

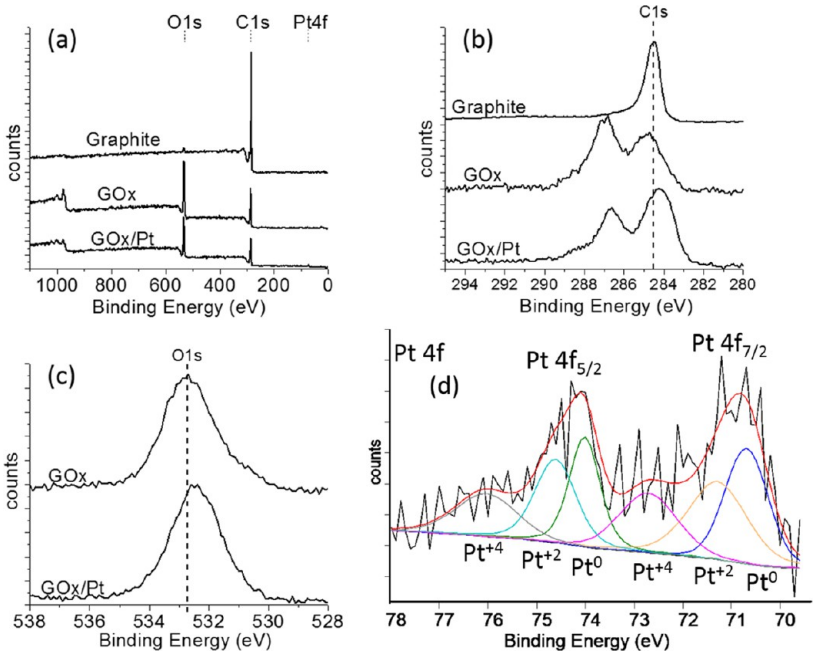

Figure 4. X-ray photoelectron spectroscopy spectra of graphite, GOx and erGOx/Pt. (a) Full binding energy spectrum and (b) C1s, (c) O1s, and (d) deconvoluted Pt4f binding energy region.

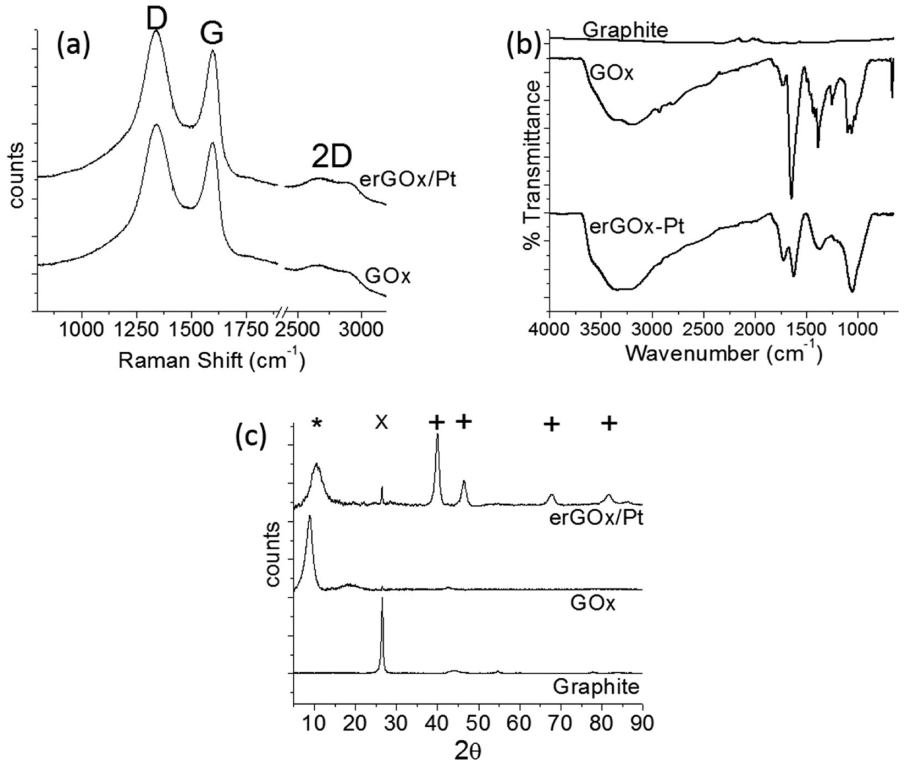

Figure 5. Characterization of graphite, GOx, and erGOx/Pt in (a) Raman spectroscopy, (b) attenuated total reflection FT-IR, and (c) X-ray diffraction.

3.3.3. Attenuated Total Reflectance Fourier Transform Infrared Spectroscopy (ATR FT-IR). ATR FT-IR spectra of Graphite, GOx and erGOx/Pt are shown in Figure 5b where the broad peak between 2000 and 3700 cm^{-1} in GOx and erGOx/Pt is attributed to the O—H bonds in the layers as well as the water adsorbed in GOx and erGOx/Pt samples. In the case of GOx, the absorption bands at 1732, 1251, and 1099 cm^{-1} are typical of the carbon−oxygen moieties reported before for the spectra of GOx. The peak at 1645 cm^{-1} can correspond to vibrations of adsorbed water molecules and C═C bonds. The main difference in erGOx/Pt is the smaller absorption peak at 1622 cm^{-1}, which may be due to the electrochemical reduction and lower amount of adsorbed water molecules.[31]

3.3.4. XRD. The syntheses of GOx and erGOx/Pt were also studied by XRD, as shown in Figure 5c. Graphite shows a sharp

dx.doi.org/10.1021/am4052552 | ACS Appl. Mater. Interfaces 2014, 6, 2137−2145

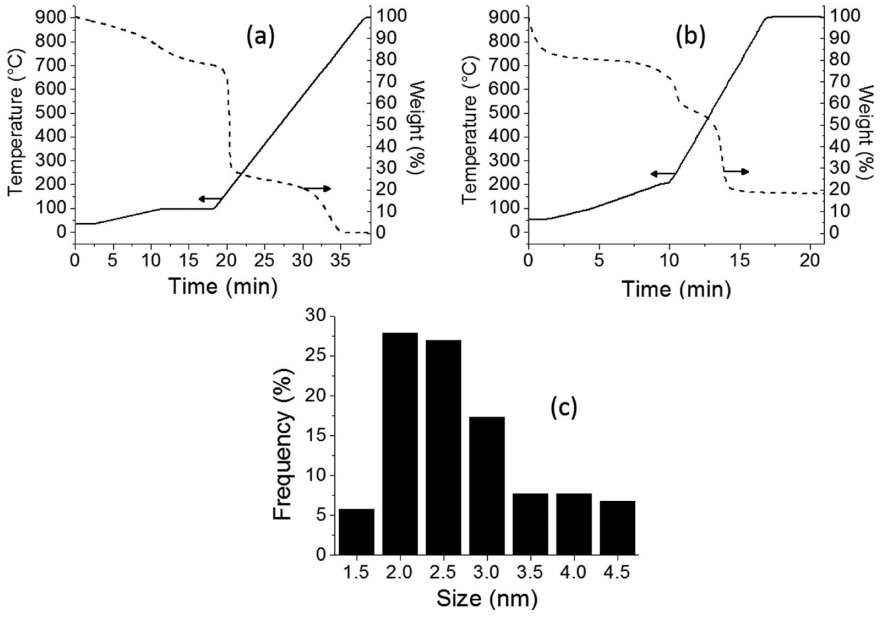

Figure 6. Characterization of GOx and erGOx/Pt using (a, b) thermogravimetric analysis and (c) histogram of nanoparticle size distribution.

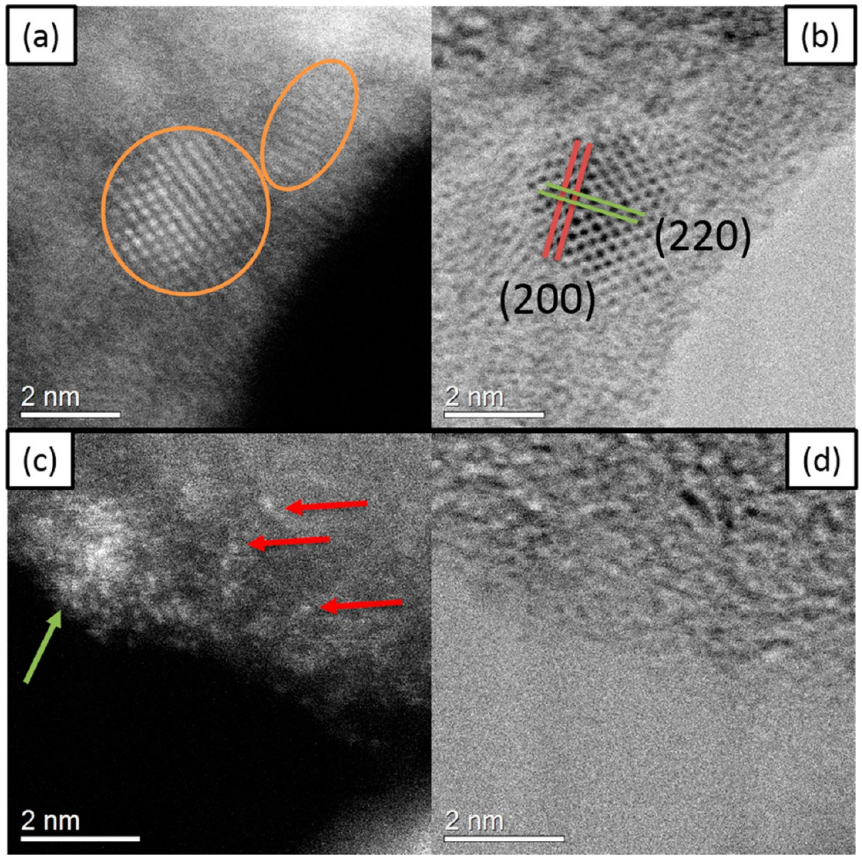

Figure 7. High resolution scanning transmission electron microscopy images of erGOx/Pt showing (a, b) Pt nanoparticles and (c, d) Pt clusters and atoms.

peak (×) at 26.59°, corresponding to the (200) peak of 0.335 nm interplanar distance. In GOx, this peak is displaced due to the exfoliation and disruption of the graphite (200) space introducing oxygen species. The addition of these carbon−oxygen moieties separate the planes and displace the (200) peak at a lower angle with a big broad peak (*) at 8.85°, which corresponds to an interplanar distance of about 1 nm. The synthesis of erGOx/Pt displaces the (200) peak to higher angle, a broad peak at 10.60°, and a sharp peak at 26.48°. These peaks correspond to interplanar distances of 0.83 and 0.336 nm, respectively. These changes are due to the electrochemical reduction of GOx during the synthesis of erGOx/Pt. Moreover, four more peaks appear (+), which correspond to the crystalline structure of Pt. Using Sherrer's equation,[32] crystallite

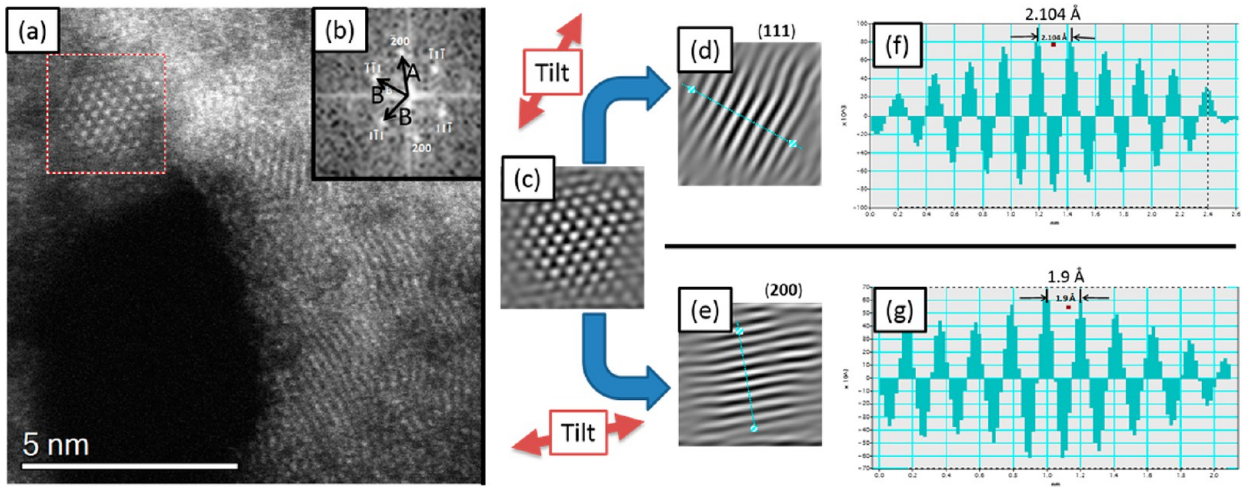

Figure 8. High resolution scanning transmission electron microscopy image of (a) erGOx/Pt nanoparticle, (b) the FFT, (c) filtered image, and the (d and f) (111) and (e and g) (200) interplanar distance analyses.

size was estimated at about 9 nm, which suggests the synthesis of Pt nanoparticles together with the deposition of Pt atoms and clusters in GOx.

3.3.5. Thermogravimetric Analysis (TGA). To know the Pt loading in erGOx/Pt and the amount of humidity in the samples, TGA was performed in air. Figure 6a,b shows the TGA of GOx and erGOx/Pt samples, where it is shown that they had about 23% and 20% of water adsorbed, respectively. After that, the labile oxygen functional groups will evaporate to carbon oxide gas species, which is followed by the oxidation of the carbon left by the high temperature in air. GOx finished at 0% after reaching 1000 °C, whereas erGOx/Pt stayed at 18.4%, the Pt loading. The smaller drop in weight for the erGOx/Pt compared to GOx between 200 and 300 °C is due to the electrochemical reduction, which lowered the amount of carbon−oxygen in erGOx/Pt.

3.3.6. HRTEM and HRSTEM. HRTEM and HRSTEM were used to determine the morphology of the synthesis. Even though XRD data suggested that there were 9 nm nanoparticles, HRTEM images showed smaller particles, as seen in the histogram presented in Figure 6c. The nanoparticles measured in HRTEM had a particle size of 2.5 ± 0.8 nm. Figure 7 shows (a, c) HAADF and (b, d) BF images of the erGOx/Pt sample. Two Pt nanoparticles are shown in panel a by ovals, with the (200) and (220) planes indicated in panel b. Moreover, Pt clusters and atoms are deposited, as shown by the green and red arrows in panel c, respectively. Here HRSTEM images give a contrast that depends on the atomic number (Z) of the atom imaged, and adding aberration correction allows visualizing single atoms. The HAADF-HRSTEM image shown in panels a and c are clear evidence for the presence of isolated atoms, small clusters, and nanoparticles, which appear as white dots, which correspond to a high Z element.

Figure 8a shows an HRTEM micrograph of erGOx/Pt, where we can appreciate the atomic arrangement of Pt nanoparticles. Panel b shows the Fast Fourier Transform (FFT) of the area marked with the square over a nanoparticle. The spots in the pattern indicate that the relationship between distances A and B is close to 1.15 Å, and the angles between A−B and B−B are close to 55° and 70°, respectively. Therefore, it means that the diffractogram obtained by FFT corresponds to an FCC crystal structure and the zone axis in this case is [011].

Figure 8c shows the filtered image, which is rotated to obtain Figure 8d,e. Figure 8d is only taking reflections (111), which here can be seen the fringe spacing that corresponds to the family of planes (111). Figure 8f shows the intensity profile corresponding to the line drawn perpendicular to the planes over Figure 8d, which shows spacing between planes of 2.1 Å. Figure 8e shows the filtered image only taking reflections (200), which here can be seen the fringe spacing corresponds to the family of planes (200). Figure 8g shows the intensity profile corresponding to the line drawn perpendicular to the planes over Figure 8e, which shows spacing between planes of 1.9 Å. These d-values, 2.1 and 1.9 Å, correspond to the d-spacing reported by the Joint Committee on Powder Diffraction Standards (JCPDS) files for FCC Pt. Table 1 summarizes the measured d-values from FFT analysis, the family of planes, which corresponds to these spacing, and the error with respect to the values reported in the literature.

Table 1. d-Values from FFT Analysis and the JCPDS

hkl	measured d-value (Å)	JCPDS d-value (Å)	error (Å)
(111)	2.1	2.26	0.16 (7%)
(200)	1.9	1.96	0.06 (3%)

3.3.7. Electrochemical Analysis. The erGOx/Pt materials were analyzed electrochemically to assess the Pt RoDSE electrodeposition and its ammonia oxidation activity as compared to commercial Pt/Vulcan and polycrystalline Pt electrodes. First, the erGOx/Pt/GC sample was done by cyclic voltammetry (CV) in 0.5 M H_2SO_4 at 20 (solid), 50 (dashed) and 100 (dotted) mV/s from −0.2 to +1.1 V vs AglAgCl. As shown in Figure 9a, a classic polycrystalline Pt voltammogram is seen, confirming Pt electrodeposition at erGOx. This polycrystalline voltammetric structure can be seen by having more than one peak in the hydrogen adsorption−desorption potential region. However, the presence of a peak at about 0.02 V vs AglAgCl corresponds to the presence of a higher amount of (100) planes and terraces compared to standard Pt polycrystalline electrodes, which are highly active for ammonia oxidation. To determine its ammonia oxidation activity, the erGOx/Pt samples were used in a CV experiment in 1.0 M NH_4OH at 10 mV/s (see Figure 9b) and it was compared to a commercially available polycrystalline Pt disk electrode (BAS

dx.doi.org/10.1021/am4052552 | ACS Appl. Mater. Interfaces 2014, 6, 2137−2145

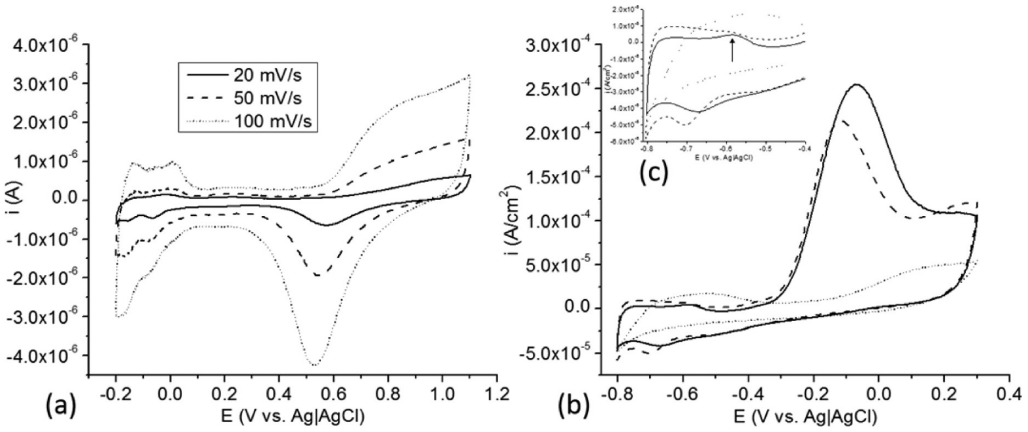

Figure 9. Cyclic voltammetry of erGOx/Pt in (a) 0.5 M H_2SO_4 at 20 (solid), 50 (dashed), and 100 (dotted) mV/s, in (b) 1 M NH_4OH at 10 mV/s (solid) vs Pt disk (dashed) and Vulcan/Pt 20% (dotted), and (c) hydrogen adsorption−desorption potential region expansion.

Inc.) and commercially available Vulcan/Pt 20% (E-TEK) without pretreatment. The currents were normalized by Pt active surface area, as determined by the charge under the peaks seen in the hydrogen adsorption−desorption potential region. The onset of the oxidation of ammonia was at ca. −0.3 V vs Ag|AgCl for erGOx/Pt/GC and Pt polycrystalline disk electrode, compared to the onset in Vulcan/Pt catalysts materials, which was at ca. 0.0 V vs Ag|AgCl. Clearly, Vulcan/Pt catalysts was deactivated out of the bottle, which means that its use for fuel cell preparations should include an activation step that is not needed with our electrocatalyst. The oxidation current is more than five times higher for erGOx/Pt compared against Vulcan/Pt, and more than 20% higher than that for a polycrystalline Pt disk electrode.

The higher peak current activity shown by erGOx/Pt may be explained by the higher amount of (100) facets and terraces that can also be seen in Figure 9c cyclic voltammogram hydrogen adsorption−desorption potential region at ca. −0.58 V vs Ag|AgCl, in comparison with the Pt disk electrode that shows a smaller peak current density. J. Feliu and collaborators[28] have shown experimentally that a higher amount of (100) facets and terraces associated with this peak correlates with higher ammonia oxidation peak current densities. Moreover, D. Skachkov and collaborators[33] studied the oxidation of ammonia in Pt using combined first principle molecular dynamics and density functional theory, and explained that Pt (100) facets have a high activity in the oxidation of ammonia because they allow N, NH and NH_2 intermediates to adsorb to two Pt atoms by forming a bridging nitrogen, which continue to N_2 formation. However, Pt (111) and (110) surfaces are inactive due to poisoning by the strong adsorption of nitrogen at hollow sites, preventing the reaction to continue due to the high activation energy barrier to overcome this.

4. CONCLUSIONS

Graphene oxide nanolayers of up to 250 nm wide were synthesized with the aim of having a higher dispersion in aqueous solutions. The highly oxidized graphene was used unsupported for the electrodeposition of Pt nanoparticles, clusters and atoms by the rotating disk slurry electrode technique. To the best of our knowledge, there is no method for the electrodeposition of metal nanoparticles/clusters/atoms on unsupported GOx, because it has been done on GOx modified conductive electrodes. In the RoDSE technique, during the Pt electrodeposition, the unsupported GOx is reduced without the need of any polluting reducing reagent, which may be a "greener" scalable process way to reduce GOx. Moreover, the synthesized erGOx/Pt nanomaterial showed enhanced peak current densities and catalytic activity for the oxidation of ammonia when compared to commercial Pt/Vulcan and polycrystalline Pt electrodes, which may be due to the electrodeposition process of highly dispersed Pt nanoparticles/clusters/atoms as was shown in the HRSTEM images. This may include a higher density of Pt(100) facets and terraces.

AUTHOR INFORMATION

Corresponding Author

*C. R. Cabera. Tel.: +1-787-764-0000 (ext. 4807). Fax: +1-787-756-8242. E-mail: carlos.cabrera2@upr.edu.

Notes

The authors declare no competing financial interest.

ACKNOWLEDGMENTS

The research work was supported in part by NASA-URC Grant No. NNX10AQ17A. Financial support of the NSF-NSEC Center for Hierarchical Manufacturing Grant No. CHM-CMMI-0531171 is also gratefully acknowledged. We also thank Sahas Rathi and Dr. Hsu from the University of Massachusetts at Amherst for the Raman spectra. The authors acknowledge the support of the following institutions and projects: NSF: The National Science Foundation grant award # DMR-1103730, "Alloys at the Nanoscale: The Case of Nanoparticles, Second Phase"; NIH−RCMI: RCMI grant 5G12RR013646-12; the National Center for Research Resources (5G12RR013646-12); the National Institute on Minority Health and Health Disparities (G12MD007591) from the National Institutes of Health; the NSF−PREM, through the NSF PREM Grant No. DMR 0,934,218, "Oxide and Metal Nanoparticles−The Interface between Life Sciences and Physical Sciences". L.C. acknowledges the Graduate Research Fellowship from NSF-EPSCoR Institute for Functional Nanomaterials (IFN) through the Grant No. EPS-1002410.

REFERENCES

(1) Hummers, J. W.; Offeman, R. *J. Am. Chem. Soc.* **1958**, *80*, 1339.
(2) Novoselov, K. S.; Geim, A. K.; Morozov, S. V.; Jiang, D.; Zhang, Y.; Dubonos, S. V.; Grigorieva, I. V.; Firsov, A. A. *Science* **2004**, *306*, 666.

(3) Novoselov, K. S.; Jiang, D.; Schedin, F.; Booth, T. J.; Khotkevich, V. V.; Morozov, S. V.; Geim, A. K. *Proc. Natl. Acad. Sci. U. S. A.* **2005**, *102*, 10451.
(4) Bong, S.; Kim, Y. R.; Kim, I.; Woo, S.; Uhm, S.; Lee, J.; Kim, H. *Electrochem. Commun.* **2010**, *12*, 129.
(5) Antolini, E. *Appl. Catal., B* **2009**, *88*, 1.
(6) Schedin, F.; Geim, A. K.; Morozov, S. V.; Hill, E. W.; Blake, P.; Katsnelson, M. I.; Novoselov, K. S. *Nat. Mater.* **2007**, *6*, 652.
(7) Soldano, C.; Mahmood, A.; Dujardin, E. *Carbon* **2010**, *48*, 2127.
(8) Park, S.; Dikin, D. A.; Nguyen, S. T.; Ruoff, R. S. *J. Phys. Chem. C* **2009**, *113*, 15801.
(9) Marcano, D. C.; Kosynkin, D. V.; Berlin, J. M.; Sinitskii, A.; Sun, Z. Z.; Slesarev, A.; Alemany, L. B.; Lu, W.; Tour, J. M. *ACS Nano* **2010**, *4*, 4806.
(10) Lu, G. H.; Ocola, L. E.; Chen, J. H. *Nanotechnology* **2009**, *20*, 445502.
(11) Eda, G.; Fanchini, G.; Chhowalla, M. *Nature Nanotechnol.* **2008**, *3*, 270.
(12) Cunci, L.; Rao, C. V.; Velez, C.; Ishikawa, Y.; Cabrera, C. R. *Electrocatalysis* **2013**, *4*, 61.
(13) Seger, B.; Kamat, P. V. *J. Phys. Chem. C* **2009**, *113*, 7990.
(14) Dao, V. D.; Hoa, N. T. Q.; Larina, L. L.; Lee, J. K.; Choi, H. S. *Nanoscale* **2013**, *5*, 12237.
(15) Pruneanu, S.; Pogacean, F.; Biris, A. R.; Coros, M.; Watanabe, F.; Dervishi, E.; Bins, A. S. *Electrochim. Acta* **2013**, *89*, 246.
(16) Zhang, F.; Hou, C. Y.; Zhang, Q. H.; Wang, H. Z.; Li, Y. G. *Mater. Chem. Phys.* **2012**, *135*, 826.
(17) Metin, O.; Kayhan, E.; Ozkar, S.; Schneider, J. J. *Int. J. Hydrogen Energy* **2012**, *37*, 8161.
(18) Guo, J.; Wang, R. Y.; Tjiu, W. W.; Pan, J. S.; Liu, T. X. *J. Hazard. Mater.* **2012**, *225*, 63.
(19) Xin, Y. C.; Liu, J. G.; Zhou, Y.; Liu, W. M.; Gao, J. A.; Xie, Y.; Yin, Y.; Zou, Z. G. *J. Power Sources* **2011**, *196*, 1012.
(20) Kundu, P.; Nethravathi, C.; Deshpande, P. A.; Rajamathi, M.; Madras, G.; Ravishankar, N. *Chem. Mater.* **2011**, *23*, 2772.
(21) Hilder, M.; Winther-Jensen, B.; Li, D.; Forsyth, M.; MacFarlane, D. R. *Phys. Chem. Chem. Phys.* **2011**, *13*, 9187.
(22) Santiago, D.; Rodriguez-Calero, G. G.; Rivera, H.; Tryk, D. A.; Scibioh, M. A.; Cabrera, C. R. *J. Electrochem. Soc.* **2010**, *157*, F189.
(23) Contes-de Jesus, E.; Santiago, D.; Casillas, G.; Mayoral, A.; Magen, C.; Jose-Yacaman, M.; Li, J.; Cabrera, C. R. *J. Electrochem. Soc.* **2013**, *160*, H98.
(24) Santiago, D.; Rodriguez-Calero, G. G.; Palkar, A.; Barraza-Jimenez, D.; Galvan, D. H.; Casillas, G.; Mayoral, A.; Jose-Yacaman, M.; Echegoyen, L.; Cabrera, C. R. *Langmuir* **2012**, *28*, 17202.
(25) Vidal-Iglesias, F. J.; Solla-Gullon, J.; Montiel, V.; Feliu, J. M.; Aldaz, A. *J. Phys. Chem. B* **2005**, *109*, 12914.
(26) Maaref, A.; Barhoumi, H.; Rammah, M.; Martelet, C.; Jaffrezic-Renault, N.; Mousty, C.; Cosnier, S. *Sens. Actuators, B* **2007**, *123*, 671.
(27) Gerischer, H.; Mauerer, H. A. *J. Electroanal. Chem.* **1970**, *25*, 421.
(28) Vidal-Iglesias, F. J.; Solla-Gullon, J.; Feliu, J. M.; Baltruschat, H.; Aldaz, A. *J. Electroanal. Chem.* **2006**, *588*, 331.
(29) Cunci, L.; Cabrera, C. R. *Electrochem. Solid-State Lett.* **2011**, *14*, K17.
(30) Luo, J. Y.; Cote, L. J.; Tung, V. C.; Tan, A. T. L.; Goins, P. E.; Wu, J. S.; Huang, J. X. *J. Am. Chem. Soc.* **2010**, *132*, 17667.
(31) Venugopal, G.; Krishnamoorthy, K.; Mohan, R.; Kim, S. J. *Mater. Chem. Phys.* **2012**, *132*, 29.
(32) Patterson, A. L. *Phys. Rev.* **1939**, *56*, 978.
(33) Skachkov, D.; Rao, C. V.; Ishikawa, Y. *J. Phys. Chem. C* **2013**, *117*, 25451.